NASA Contractor Report 190791
AIAA–92–3462

Scaling of 100 kW Class Applied-Field MPD Thrusters

Roger M. Myers
Sverdrup Technology, Inc.
Brook Park, Ohio

Prepared for the
28th Joint Propulsion Conference and Exhibit
cosponsored by the AIAA, SAE, ASME, and ASEE
Nashville, Tennessee, July 6–8, 1992

NASA

Scaling of 100 kW Class Applied-Field MPD Thrusters

Roger M. Myers[1]
Sverdurp Technology, Inc.
NASA Lewis Research Center Group
Brook Park, OH 44142

Abstract

Three cylindrical applied-field magnetoplasmadynamic thrusters were tested with argon propellant over a broad range of operating conditions to establish empirical scaling laws for thruster performance. Argon flow rates, discharge currents, and applied-field strengths were varied between 0.025 and 0.14 g/s, 750 to 2000 A, and 0.034 to 0.20 T, respectively. The results showed that the thrust reached over five times the self-field value, and that thrust increased linearly with the product of discharge current and applied-field strength and quadratically with the anode radius. While increasing the propellant flow rate increased the thrust, it did not affect the rate of thrust increase with applied-field strength, and at low propellant flow rates the self-field thrust approached 30% of the measured thrust. The voltage increased linearly with applied-field strength but was insensitive to the discharge current. The rate of voltage increase with applied-field strength was strongly dependent on anode radius. Thruster efficiency increased monotonically with applied-field strength and propellant flow rate. Peak thruster efficiencies were insensitive to changes in anode radius. Electrode power loss and thruster efficiency measurements showed that while the electrode losses decreased with increasing anode radius the plasma losses increased. The opposite behaviors of electrode and plasma losses demonstrates the need to identify ways of independently controlling the thruster loss mechanisms.

Nomenclature

b	self-field thrust coefficient, N/A^2
B_z	applied magnetic field strength, T
e	electron charge, C
g	acceleration of gravity, m/s^2
I_{sp}	specific impulse, s
J_d	discharge current, A
k	Boltzmann's constant, J/K
$\dot{m}$	mass flow rate, g/s
L_a	anode length, m
L_c	cathode length, m
P_i	ionization power, W
P_r	power radiated to anode surface, W
P_{conv}	power convected to anode surface, W
R_a	anode radius, m
R_c	cathode radius, m
T	thrust, N

[1]Propulsion engineer, member AIAA

T_{sf}	self-field thrust, N
T_e	electron temperature, K
V_a	anode fall voltage, V
V_d	discharge voltage, V
η	efficiency
η_{th}	thermal efficiency
η_f	flow efficiency
μ_o	permeability of free-space
Φ	anode work function, eV

Introduction

Magnetoplasmadynamic (MPD) thrusters have demonstrated performance and power handling capabilities which make them attractive for use as primary propulsion on piloted and robotic planetary and near-Earth missions.[1,2] Thruster efficiency and specific impulse have reached over 40 percent and 5000 seconds, respectively, and steady-state thrusters have been tested at power levels ranging from 30 - 500 kW.[3] While piloted planetary missions will likely require power levels between one and ten megawatts, there is potential for nearer term application of 100 kW class thrusters for robotic missions. In addition, facility limitations preclude immediate testing of multimegawatt steady-state thrusters,[4] forcing the development of detailed scaling models at submegawatt power levels.

A typical laboratory MPD thruster, shown schematically in Fig. 1, consists of a central, rod shaped cathode with a coaxial, cylindrical anode. Propellant, injected through the insulating backplate, is heated, ionized, and accelerated by the discharge current passing from anode to cathode and it's interactions with both the self-induced and externally applied magnetic fields. MPD thruster research to date has focussed on self-field devices, wherein the accelerating magnetic field is generated by the thruster discharge current.[3] However, the demonstrated performance levels of these devices at the power levels of interest is very poor, typically ranging between 5 and 10 percent efficiency at specific impulses between 800 and 1500 seconds. Recent work has shown that application of a solenoidal magnetic field to the thruster chamber increases the thruster performance in proportion to the strength of the applied magnetic field.[3,5] Efficiencies between 20 and 25 percent at specific impulses between 1500 and 4000 seconds have been demonstrated.[5] A systematic study of the effect of electrode geometry showed that, for a constant argon flow rate of 0.1 g/s and a discharge current of 1000 A, the discharge voltage and thrust increased quadratically with the anode radius, linearly with applied-field strength, and inversely with the cathode radius.[5] However, that work did not address the effect of either the propellant flow rate or the discharge current.

The purpose of this work is to develop applied-field MPD thruster scaling laws including the effects of thruster geometry, applied magnetic field strength, propellant flow rate, and discharge current. The effect of varying the discharge current and propellant flow rate was studied for three of the geometries studied in Ref. 5. The need to include several geometries is apparent from the complex coupling of plasma heating, ionization, and acceleration phenomena occuring in MPD thrusters. That is, the effect of operating condition on thruster performance is likely to depend on the thruster geometry. Following a description of the thrusters and experimental facility, performance measurements for the three applied-field MPD thruster geometries shown in Fig. 1 are given for the operating conditions listed above. These measurements are then used to establish scaling laws for voltage, thrust, specific impulse, and efficiency which are applicable to applied-field thrusters operated in the 100 kW power range. In addition, the data are compared with existing analytical models to establish dominant acceleration and power loss mechanisms. These results will not only serve as a guide for future experimental research, but will also be useful as a data base with which to compare the results of numerical simulations.

Experimental Apparatus and Procedures

Thruster and Magnet Assembly

All MPD thrusters tested consisted of a 0.64 cm radius, 7.6 cm long 2% thoriated tungsten cathode surrounded by a coaxial 7.6 cm long copper anode. Three anode radii, 2.54, 3.81, and 5.1 cm, were tested. As shown schematically in Fig. 1, both electrodes were water cooled, the anode via azimuthal passages in the wall, the cathode via conduction up the base to a copper cathode clamp. Propellant was injected through a boron nitride backplate via an 0.16 cm wide annulus surrounding the cathode and twenty-four 0.16 cm diameter holes at the mid-radius between the cathode and anode. All gas seals were made using 0.05 cm thick graphite gaskets.

The thrusters were inserted into a 15.3 cm long solenoid for testing with an applied magnetic field. Two magnet bore radii, 15.3 cm and 20.3 cm, were required to accommodate the three anode radii. The smaller magnet was used with the 2.54 cm and 3.81 cm radius anodes, and the larger with the 7.6 cm anode. Magnetic field strength calibrations showed that both magnets produced azimuthally uniform fields, with magnitudes of 1.66×10^{-4} T/A and 8.48×10^{-5} T/A at the centerline of the magnet exit plane (also the thruster cathode tip) for the 15.3 cm and 20.3 cm magnets, respectively.

Facility and Test Support Equipment

The MPD thruster test stand, shown in Fig. 2, was mounted in a 3 m diameter, 3 m long test port attached to the main 7.6 m diameter, 21 m long vacuum tank via a 3 m diameter gate valve. The main chamber was pumped by twenty 0.9 m diameter oil diffusion pumps backed by three roots blowers and two roughing pumps. The facility pressure was kept below 0.07 Pa (5×10^{-4} torr) during testing, which is low enough to ensure that ambient gas entrainment did not affect the performance measurements.[5]

Thruster power was provided by a series-parallel ladder network of six welding supplies with an output capability of up to 3000 A at 130 V. The applied-field magnet was powered by a single welding supply providing up to 1500 A to the coil. Both supplies were isolated from ground. A 1400 V pulse applied between anode and cathode was used to ignite the arc. Discharge voltage and current ripple was approximately 20% at a frequency of about 600 Hz.

Cooling water was supplied to both the thruster and magnet using two closed loop heat exchangers, each providing up to 0.47 l/sec. The water flow rate was measured using turbine flow meters which were calibrated at regular intervals during the testing.

Propellant flow rates were measured using thermal conductivity type flow controllers with 2% precision. A constant volume calibration system was regularly used to obtain an absolute measure of gauge accuracy. The calibrations showed the propellant feed rates to be accurate to within 2%.

Thruster performance was determined from measurements of thrust, propellant flow rate, discharge power, and electrode heat transfer. Thrust was measured using an inverted pendulum thrust stand with an oscillation damping circuit, remote leveling apparatus, and an in situ calibration mechanism. As discussed in Ref. 5 and 6, extensive calibration and testing showed the thrust stand error was less than 3%. Thruster discharge current was measured using both shunts and Hall effect transducers. Current and voltage were continuously displayed on a set of panel meters and simultaneously fed into a computerized data acquisition system. The electrode heat transfer was measured calorimetrically by monitoring the cooling water temperature change and flow rate. Both of these measurements were calibrated several times during the test series. The water flow rates were accurate to within 2%,

and the temperature rise to within +/- 0.5 °C. Due to the different temperature rises occuring across the anode and cathode cooling channels and the strong dependence of the temperature rise on operating condition, the electrode power measurement accuracy had to be calculated for each operating condition, though it typically was 3% for the anode and 20% for the cathode.

Performance Measurements

Specific impulse, efficiency, thermal efficiency, and flow efficiency were used as measures of thruster performance. The specific impulse and efficiency, sometimes referred to as thrust efficiency, were calculated from:

$$I_{sp} = \frac{T}{\dot{m}g} \qquad \eta = \frac{T^2}{2\dot{m}V_d J_d} \tag{1}$$

and the thermal and flow efficiencies were obtained from:

$$\eta_{th} = 1 - \frac{P_a + P_c}{V_d J_d} \qquad \eta_f = \frac{\eta}{\eta_{th}} \tag{2}$$

The thermal efficiency is the fraction of the input power which is deposited into the plasma, and the flow efficiency is a measure of the fraction of the power deposited into the plasma that is converted to thrust power. The experimental measurement of thermal efficiency does not include power radiated from the cathode surface which escaped through the exit plane, though it does include the fraction of this power which is absorbed by the anode. The magnitude of this omission was estimated to be less than 3 kW by assuming that the entire discharge current was thermionically emitted from the cathode to estimate the cathode surface temperature and using the known view factors for cylindrical chambers.[7] Power absorbed by the boron nitride backplate is included in the thermal efficiency because the backplate is cooled by conduction to both the cathode clamp and the anode (Fig. 1). These assumptions yield a flow efficiency which is lower than the true value.

The voltage drop across the plasma was calculated by estimating the anode fall voltage and subtracting it from the total measured discharge voltage. The anode fall voltage was estimated using the standard model for anode power deposition:[8,9]

$$P_a = J_d\left(V_a + \frac{5kT_e}{2e} + \Phi\right) + P_r + P_{conv} \tag{3}$$

where the first term represents the contribution of the current carrying electrons, the second represents radiation from the plasma and cathode, and the third term accounts for convective heat transfer from the hot flowing plasma. Gallimore et al.[10] and Myers et al.[9] showed that the dominant contributions to anode power were the first and second terms, and that the cathode was the dominant source of radiant heat. Thus, the anode fall was calculated by subtracting the estimated cathode radiation contribution from the calorimetrically measured anode power, dividing by the discharge current, and subtracting 9.6 volts to account for the copper work function (4.6 V) and the electron thermal energy (with Te = 2 eV).[9] The plasma voltage drop was then estimated as the difference between the discharge voltage and the anode fall voltage. The cathode fall voltage has been shown to be small for thermionically emitting cathodes in MPD thrusters.[11,12]

Experimental Results

Thruster performance measurements were attempted for the three anode radii at argon propellant flow rates of 0.05, 0.10, and 0.14 g/s, and at discharge currents of 750, 1000, 1250, 1500, and 2000 A as a function of applied magnetic field strength. However, it was not possible to obtain steady operation at all operating conditions due to either the onset of severe electrode erosion (evidenced by particulate emission) or limitations on the flow rate of the electrode cooling water. In addition, attempts to operate without an applied-field always resulted in unstable operation leading quickly to meltdown of the anode. In general, as the thruster size increased the propellant flow rate had to be increased to maintain the same discharge current and applied-field strength range. Thus, the largest stable operating range was observed with the 2.54 cm anode radius thruster operating at 0.10 g/s, and the largest anode, with a 5.1 cm radius, could not be operated without severe electrode erosion at a propellant flow rate of 0.05 g/s. The peak applied-field strengths decreased from 0.20 T with the 2.54 cm radius anode to 0.062 T with the 5.1 cm radius thruster as a result of anode cooling limitations. The data presented below, organized according to performance parameter, are limited to operating conditions for which either the applied magnetic field or the discharge current could be varied by a significant amount.

Discharge and Plasma Voltages

The effect of applied magnetic field strength and discharge current on the discharge voltage for the 2.54, 3.81, and 5.1 cm anode radii is shown in Figs. 3a - c. For all cases the voltage increased nearly linearly with applied field strength, but the dependence on discharge current was not monotonic, and the effect of anode radius was much larger than the effect of current level. Discharge voltages ranged from approximately 20 V with the 2.54 cm radius thruster at the lowest applied field strength, to over 100 V with the 5.1 cm radius thruster with the highest applied-field that could be used with that geometry. The effects of current level and anode radius are more clearly shown in Table 1, which lists the slopes of the least-squares curve-fits to the discharge voltage vs. applied field strength plots. Doubling the discharge current with the smallest anode radius thruster barely changed the V_d vs. B_z slope, but doubling the anode radius increased the slope by as much as a factor of five. It was not possible to establish the quantitative dependence of the V_d vs. B_z slope on either anode radius or current level. Increasing the discharge current by 250 A generally increased the discharge voltage by between 2 and 10 V, with the magnitude of the effect increasing with anode radius. The anomalous discharge voltage behavior observed with the 5.1 cm radius anode at a discharge current of 750 A resulted from a change in anode fall voltage.[9] To eliminate the superposition of anode and plasma phenomena, plasma voltage drops were calculated using the procedure described above. Plasma voltage drop estimates are shown in Figs. 4a - c for the same conditions described in Fig. 3, and the slopes of the curves are given in Table 2. The results clearly show the large impact of the anode fall voltage. While the plasma voltage drop increased linearly with applied field strength, the magnitudes were significantly below those of the discharge voltage. The lowest plasma voltage drop was below 20 V and the highest was only 60 V. The rate of increase in plasma voltage drop with applied field, given in Table 2, is over a factor of two below the rate of rise of the discharge voltage, given in Table 1, for all operating conditions tested. In contrast to the results for the discharge voltage, both the magnitudes and slopes of the plasma drops for the different current levels are nearly the same, with only a slight increase in slope with increasing discharge current. It is clear that a large fraction of the effect observed on the discharge voltage resulted from changes in the anode fall voltage. The effect of geometry was still quite large, with the plasma voltage drop for the 5.1 cm anode 20 V higher than that for the 2.54 cm anode. The slopes for the plasma voltage drop vs. applied field strength results are given in Table 2. While the slopes increased rapidly with anode radius, no clear relationship could be identified between the slopes of the plasma voltage drop vs. applied-field strength and the anode radius for all discharge currents. This result contrasts with that presented in a previous work,[5] where a quadratic increase of discharge voltage with anode radius was reported.

To further characterize the effect of discharge current on the discharge and plasma voltage drops, a series of tests were conducted at a constant applied field strength of 0.033 T. The results are shown in Figs. 5a and 5b.

Increasing the discharge current from 750 A to 2000 A resulted in a 5 V rise in discharge voltage with the 2.54 cm anode, but the plasma voltage drop did not rise at all. Similar trends are evident for the other anode sizes. The data show that the dominant effect of increasing the discharge current was to slightly increase the anode fall voltage, an effect discussed in detail in Ref. 9. The voltage rise with anode radius was large, though the quantitative relationship was not apparent.

The effect of argon propellant flow rate on the discharge voltage for a discharge current of 1000 A is shown in Figs. 6a - c for the 2.54, 3.81, and 5.1 cm radius anodes, respectively. The discharge voltage magnitude and rate of increase with applied field strength increased with decreasing propellant flow rate, though the behavior changed with anode radius. For the 2.54 and 3.81 cm radius anodes the V_d vs. B_z slopes increased rapidly with decreasing flow rate, but this is not observed with the 5.1 cm radius anode. The sensitivity of the plasma voltage drop vs. magnetic field slope to the mass flow rate, shown in Fig. 7a - c for the three anodes, was much smaller. This result is confirmed by comparison of Figs. 8a and 8b, which show the discharge and plasma voltage drops as functions of the discharge current for two mass flow rates with the 5.1 cm radius anode. While the discharge voltage (Fig. 8a) increased approximately inversely with the mass flow rate, the rate of increase of the plasma voltage drop was much smaller. These results reemphasize the importance of the anode fall voltage in the voltage scaling characteristics of cylindrical 100 kW applied-field MPD thrusters.

Thrust and Specific Impulse

Thrust measurements as a function of applied magnetic field strength for discharge currents from 750 to 1500 A are shown in Figs. 9a - c for the 2.54, 3.81, and 5.1 cm radius anodes, respectively. Slopes for all least-squares curve fits are given in Table 3. The data show that for these flow rates the thrust increased approximately linearly with discharge current and quadratically with anode radius. The effect of propellant flow rate on thrust behavior is shown in Figs. 10 a - c. For the smaller anode radius there was a substantial increase in thrust as the propellant flow rate increases, though this effect diminishes for the larger thrusters. The rate of increase in thrust with applied field strength was not significantly affected by the mass flow rate. This behavior changed, however, when the discharge current and flow rate were varied for constant applied field. As shown in Fig. 11a, for the 2.54 cm radius anode with a flow rate of 0.05 g/s the thrust increased quadratically, not linearly, with discharge current. The self-induced magnetic field thrust, calculated from:[13]

$$T_{sf} = \frac{\mu_o J_d^2}{4\pi} \ln\left(\frac{R_a}{R_c}\right) \qquad (4)$$

is also shown on the figure, and it is clear that it contributed significantly to the thrust levels at the lower propellant flow rate. The quadratic behavior disappeared with either increasing mass flow rate or increasing anode radius due to the relatively smaller contribution of the self-field thrust. This is clearly shown in Fig. 11b, where the thrust for the 5.1 cm radius anode is plotted as a function of the discharge current for two argon flow rates. For this case the self-field thrust was always less than 25% of the measured thrust, and for low discharge currents its contribution dropped to less than 10%.

The small effect of propellant flow rate on the rate of increase in thrust with applied field strength clearly results in an inverse relationship between the specific impulse, defined by Eq. (1), and the flow rate. For the data shown, a maximum specific impulse of 1900 s was obtained with the smallest anode radius at a propellant flow rate of 0.05 g/s. Testing with this anode at a propellant flow rate of 0.025 g/s at a discharge current of 750 A yielded a maximum I_{sp} of 2400 s.[5]

Efficiency

Efficiency measures the combined effects of the thrust and discharge voltage dependencies on geometry and operating condition. Results are shown as a function of applied-field strength for three discharge currents using the 2.54 cm, 3.81 cm, and 5.1 cm radius anodes in Figs. 12a - c. The increase in propellant flow rate for the larger thruster was required to achieve stable operation over the desired discharge current range. For all cases the efficiency increased approximately linearly with applied magnetic field strength. As shown in Fig. 12a, the maximum efficiency for the small anode was measured with 1000 A discharge. This was not true for either of the larger anode radii, for which the efficiency increased monotonically with discharge current. This difference is more clearly shown in Figs. 13a and b, in which the efficiencies for the 2.54 and 5.1 cm radius anodes are plotted as a function of discharge current for a constant applied field strength of 0.034 T and two argon flow rates. While the efficiency for both the 2.54 cm and 5.1 cm radius anodes increased with propellant flow rate, the dependence on discharge current changed with anode size. For the smaller anode at 0.10 g/s there was a maximum efficiency at a discharge current of ~ 1100 A, above which the efficiency decreased slightly, however, efficiency increased monotonically with discharge current at the lower flow rate. With the large anode the efficiency increase with current was unaffected by propellant flow rate.

The effect of propellant flow rate on the efficiency response to applied-field strength is shown in Figs. 14a - c for the three anode radii. The effect of flow rate is quite large with the small anode, with an increase from 0.08 to 0.20 when the flow was increased from 0.05 to 0.10 g/s at low applied-field strengths (Fig. 14a). By contrast, the same flow increase with the 3.81 cm anode had a negligible effect on efficiency (Fig. 14b), though the increased flow did increase the stable operating range of the thruster so as to achieve a higher maximum efficiency of 0.18. The effect with the largest anode (Fig. 14c) was similar, with the dominant effect of propellant flow being an increase in the stable operating range.

Flow Efficiency

The efficiency of 100 kW class MPD thrusters has been previously shown to be predominantly controlled by anode power deposition.[5,9,10] This was confirmed in this work for a much broader set of operating conditions by the large fraction of the discharge voltage which was accounted for by the anode fall voltage. While this result clearly shows the need to concentrate on reducing the anode power loss, it also indicates that changes in anode power deposition could be masking the behavior of other plasma power sinks. For this reason an attempt was made in this work to isolate the efficiency with which power deposited into the plasma was converted to directed kinetic, or thrust, power. This term, the flow efficiency, which increases as losses resulting from ionization, unrecovered rotational (swirl) and thermal energy, divergence losses, and radiation are decreased, provides a measure of potential thruster efficiency if anode losses can be eliminated.

Results for flow efficiency, defined by Eq. (2), are shown in Figs. 15a - c for the three anode radii for several discharge currents. For the small anode (Fig. 15a) the flow efficiency first decreased with increasing applied-field strength and then increased slightly. For both of the larger anodes (Figs. 15b and c) the flow efficiency increased monotonically with applied-field strength. The maximum flow efficiency, 0.60, was obtained with the 2.54 cm radius anode at the minimum applied-field, though this value was nearly reached again at an applied-field of 0.20 T with a discharge current of 1250 A. The flow efficiency clearly decreased with increasing anode radius, with maximum values of 0.60, 0.50, and 0.45 with the 2.54, 3.81, and 5.1 cm radius anodes, respectively. The flow efficiency generally increased with increasing discharge current. The effect of propellant flow rate is illustrated in Figs. 16a and b. For the same change in propellant flow rate, the response of the 3.81 and 5.1 cm radius anodes was opposite, with the flow efficiency decreasing with increasing flow for the smaller anode, and increasing with the larger anode. For all cases the flow efficiency increased monotonically with increasing applied-field strength, though there appears to be a leveling off at the higher fields.

Discussion

The discharge voltage, plasma voltage drop, and thrust all increased linearly with applied magnetic field strength for the geometries and operating conditions tested. However, the dependencies of these parameters on flow rate, discharge current, and geometry were more complex. While the discharge voltage was not very sensitive to the discharge current for a given anode size and flow rate, changes in discharge current had a strong effect on the dependence of voltage to those parameters. Thus, in contrast to the work in Ref. 5 where a simple quadratic dependence was found between the discharge voltage and the anode radius, this work indicates a much more complex relationship in which the magnitude of the exponent depends on both the discharge current and the propellant flow rate. Note that the increase with anode radius is always faster than linear, which is the rate predicted by Fradkin using a simple homopolar generator model.[14] Only for a discharge current of 1000 A did the discharge voltage appear to increase quadratically with anode radius. Separation of the plasma voltage drop did not eliminate this problem, though it did reduce the dependence on the discharge current. The lack of sensitivity of voltage to discharge current at a given applied field strength has been observed previously in both steady-state and quasi-steady thrusters.[14-18] Increasing the propellant flow rate always decreased the discharge and plasma voltages, though again the behavior did not follow a simple power relationship.

In contrast to the voltage behavior, the thrust scaling was well defined. For propellant flow rates of 0.10 and 0.14 g/s the thrust increased as:

$$T \sim J_d B_z R_a^2 \tag{5}$$

and the discrepancy at low flow rate (see Fig. 11a) can be resolved by including the self-induced magnetic field thrust term. Self-field acceleration appears to play a substantial role in the small applied-field thruster at low applied field strengths and propellant flow rates. In addition, while the propellant flow rate did not greatly affect the thrust vs. B_z slope (Fig. 10a - c), increasing the propellant flow rate can increase the magnitude of the thrust. This results in the relation:

$$T = bJ_d^2 + B_z J_d R a^2 + f(R_a, m) \tag{6}$$

where the self-field thrust coefficient was defined in Eq. (4) and the third term indicates that the flow rate dependence was a function of anode radius. The sensitivity to propellant flow rate clearly decreased with increasing anode radius. The latter may result from a pressure thrust term, though it was not possible to prove this with the available data. At constant flow rate, the fraction of thrust arising from pressure forces would likely decrease with increasing anode radius due to the quadratic rise of the applied-field thrust. The thrust increase with $B_z J_d$ has been reported previously,[14-18] though previous work had failed to resolve the self-field acceleration and propellant flow rate dependence.

The observed lack of dependence of the geometric scaling on discharge current and flow rate indicates that it is possible to incorporate into Eq. 6 the thrust dependence on anode length, cathode radius, and cathode length established in Ref. 5. The final thrust scaling relationship is:

$$T = bJ_d^2 + \frac{R_a^2 J_d B_z}{k_1 L_c R_c} + f(L_a, R_a, \dot{m}) \tag{7}$$

where the third term now also accounts for the observation in Ref. 5 that the thrust decreased for longer anodes, but that the anode length did not affect the thrust vs. B_z slope.

While both thrust and discharge voltage rose linearly with applied field strength, the rate of thrust rise was equal to or slightly greater than that for the voltage rise, resulting in an increase in efficiency with increasing field strength. The insensitivity of the voltage to discharge current, combined with the linear rise in thrust with

discharge current, resulted in higher efficiencies for higher discharge currents. Increasing the propellant flow rate generally increased the efficiency as a result of the combined increase in thrust and decrease in discharge voltage. As discussed in Ref. 9, increasing the propellant flow rate reduced the anode power fraction, explaining in part the increased efficiency.

The high values of flow efficiency, 0.5 to 0.6, indicate that if the anode power loss can be reduced high efficiency MPD thrusters may be realizable. The behavior of the flow efficiency was complex, with discharge current and flow rate dependencies which were a function of anode radius. Only with the largest anode did the flow efficiency increase monotonically with applied-field strength and discharge current (Fig. 15c). With the smallest anode both these trends were reversed at low field strengths, and with the 3.81 cm radius anode at low field strengths the lowest discharge current resulted in the highest flow efficiency.

The decrease in flow efficiency with anode radius indicates that the magnitude of one or several of the plasma loss mechanisms is increasing. Spectroscopic studies indicate that the argon plasma is nearly fully ionized for most of the test conditions,[19] so that the ideal flow efficiency can be estimated from:

$$\eta_{f,id} = \frac{\frac{1}{2}\dot{m}I_{sp}^2 g^2}{\frac{1}{2}\dot{m}I_{sp}^2 g^2 + P_i} \tag{8}$$

where losses from unrecovered rotational energy, thermal energy, divergence, and radiation, have been neglected. Ideal and measured flow efficiencies are plotted vs. thruster specific impulse in Fig. 17. The measured values were obtained for the three anode radii tested at a discharge current of 1250 A and an argon flow of 0.10 g/s. In an attempt to identify the loss mechanism responsible for the low measured flow efficiencies, the magnitude of the lost power was estimated for the three cases shown in the figure. Subtracting the anode and cathode water cooling powers and the thrust power from the total input power for each thruster at the highest flow efficiency left 12.8, 19.3, and 30.6 kW unexplained for the 2.54, 3.81, and 5.1 cm anode radius thrusters, respectively. These large plasma power losses clearly show that the problem did not lie in the assumed ionization state, as fully ionizing 0.10 g/s of argon requires only 3.8 kW, and fully doubly ionizing the propellant stream, which spectroscopic data show was not occuring, requires only 10 kW. The power levels involved are also too large to be accounted for by thermal energy or plasma radiation,[20] though cathode surface radiation might account for as much as 7 kW.[9] While cathode radiation may reduce the plasma loss with the smallest anode to within measurement uncertainties, it clearly does not account for the large power loss with the larger anodes. For those geometries it appears that either unrecovered rotational energy or divergence losses control the frozen flow efficiency.

Anode power deposition studies reported in Refs. 5 and 9 show that increasing thruster size decreases the fractional anode power loss, resulting in a higher thermal efficiency. The thrust and flow efficiencies presented in this work show that for the geometries studied the flow efficiency decreases essentially at the same rate as the thermal efficiency increases. To achieve high efficiency operation the physics of the two efficiencies must be decoupled, so as to permit, for instance, an increase in size to reduce the anode power loss without compromising the flow efficiency.

Conclusions

Performance measurements with three 100 kW class applied-field MPD thrusters were obtained at several argon propellant flow rates, discharge currents, and applied magnetic field strengths to establish scaling relationships for discharge voltage, plasma voltage drop, thrust, efficiency, and flow efficiency. The voltage, thrust, and efficiency were found to increase linearly with applied field strength for all geometries and operating conditions. The discharge and plasma voltage drops were found to depend only slightly on the discharge current and to decrease with

increasing propellant flow rate. Thrust was found to increase linearly with discharge current for operating conditions where the applied-field thrust term dominated, and quadratically when the self-field term dominated at low propellant flow rates with the smallest anode. The propellant flow rate increased the thrust level without affecting the rate of thrust increase with applied-field strength, indicating the presence of a pressure thrust term which decreased in importance with increasing thruster size. Measurements of the flow efficiency showed that for some cases over 60% of the power deposited into the plasma was converted to thrust. Flow efficiency was found to decrease with increasing anode radius, increase with increasing propellant flow rate, and generally increase with increasing discharge current. An examination of the plasma power balance indicates that unrecovered rotational kinetic energy and divergence losses may play a dominant role in the flow efficiency. The opposite behaviors of electrode and plasma losses as a function of anode radius demonstrates the need to identify ways of independently controlling the thruster loss mechanisms.

Acknowledgements

The author would like to thank John Naglowsky, Larry Schultz, Jerry LaPlant, David Wolford, Peggy Yancer, John McAlea, Rob Butler, John Miller, Gerry Schneider, Bernard Loyer, Cliff Schroeder, David Wehrle, and Shawn Reese for their invaluable assistance during this project.

References

1. Gilland, J.H., Myers, R.M., and Patterson, M.J., "Multimegawatt Electric Propulsion System Design Considerations," AIAA Paper 90-2552, July 1990; see also NASA TM 105152.

2. Rudolph, L.K., and Ogg, G.M., "Orbit Transfer Using High Power MPD Thrusters," AIAA Paper 85-1478, July 1985.

3. Myers, R.M., Mantenieks, M.A., and LaPointe, M.R., "MPD Thruster Technology," AIAA Paper 91-3568. September 1991; see also NASA TM 105252.

4. Sovey, J.S., Vetrone, R.H., Grisnik, S.P., Myers, R.M., and Parkes, J.E., "Test Facilities for High Power Electric Propulsion," AIAA Paper 91-3499, Sept. 1991; see also NASA TM 105247.

5. Myers, R.M., "Applied-Field MPD Thruster Geometry Effects," AIAA Paper 91-2342, July 1991; see also NASA CR 187163.

6. Haag, T. W., "Thrust Stand for High-Power Electric Propulsion Devices," *Rev. Sci. Instrum.*, Vol. 62, No. 5, May 1991, pp. 1186-1191.

7. Howell, J. R., and Siegel, R., "Thermal Radiation Heat Transfer, Vol. 2," NASA SP-164, 1969.

8. Oberth, R., "Anode Phenomena in High Current Discharges," Ph.D. dissertation, Princeton University, Dec. 1970.

9. Myers, R. M., and Soulas, G. C., "Anode Power Deposition in Applied-Field MPD Thrusters," AIAA Paper 92-3463, June 1992.

10. Gallimore, A. D., Myers, R. M., Kelly, A. J., and Jahn, R. G., "Anode Power Deposition in an Applied-Field Segmented Anode MPD Thruster," AIAA Paper 91-2343. June, 1991.

11. Myers, R. M., Suzuki, N., Kelly, A. J., and Jahn, R. G., "Cathode Phenomena in a Low-Power Magnetoplasmadynamic Thruster," Journal of Propulsion and Power, Vol. 7, No. 5, Sept. - Oct. 1991, pp. 760-766.

12. Hoyer, K., and Subramanian, V., "Limits on Steady Diffuse Mode Operation of the Cathode in an MPD Thruster," AIAA Paper 89-2601, July 1989.

13. Jahn, R. G., Physics of Electric Propulsion, McGraw-Hill, New York, 1968.

14. Fradkin, D. B., "Analysis of Acceleration Mechanisms and Performance of an Applied-Field MPD Arcjet," Ph.D. dissertation, Princeton University, March 1973.

15. Bennett, S., Enos, G., John, R., and Powers, W., "Development of an Ammonia-Fueled MPD Arc Jet Thruster," AIAA Paper 67-690, Sept. 1967.

16. Tahara, H., Kagaya, Y., and Yoshikawa, T., "Hybrid MPD Thruster with Axial and Cusp Magnetic Fields," 20th Intern. Electric Propulsion Conference, IEPC 88-058, 20th International Electric Propulsion Conf., Garmisch-Partenkirchen, Germany, Oct. 1988.

17. Connolly, D.J., Sovie, R. J., and Seikel, G. R., "Performance and Diagnostics of a Water - Cooled Magnetoplasmadynamic Arc Thruster," NASA TN D-5836, May 1970.

18. Bennett, S., John, R., Enos, G, and Tuchman, A., "Experimental Investigations of the MPD Arcjet," AIAA Paper 66-239, March 1966.

19. Myers, R.M., Wehrle, D., Vernyi, M., Biaglow, J., and Reese, S., "A Preliminary Characterization of Applied-Field MPD Thruster Plumes," AIAA Paper 91-2339, July 1991; see also NASA CR 187165.

20. Myers, R.M., Parkes, J.E., and Mantenieks, M.A., "Multimegawatt MPD Thruster Design Considerations," 9th Symposium on Space Nuclear Power Systems, AIP Conf. Proc. 246, Jan. 1992; see also NASA TM 105405.

Anode Radius (cm)	Discharge Voltage vs. Bz Slope (V/T)			
	750 A	1000 A	1250 A	1500 A
2.54	282	274	276	298
3.81	435	655	540	
5.1	2000	1141	1239	

Table 1 - Discharge voltage vs. applied field strength slopes for 3 anode radii and 4 discharge currents. Argon flow rate of 0.10 g/s.

Anode Radius (cm)	Plasma Voltage Drop vs. Bz Slope (V/T)			
	750 A	1000 A	1250 A	1500 A
2.54	137	143	128	131
3.81	197	285	270	
5.1	494	646	735	

Table 2 - Discharge -anode fall voltages vs. applied-field strength slopes for 3 anode radii and 4 discharge currents. Argon flow rate of 0.10 g/s.

Anode Radius (cm)	Thrust vs. Bz Slope (N/T)			
	750 A	1000 A	1250 A	1500 A
2.54	4.2	6.0		7.6
3.81	9.3	13.0	15.1	
5.1	17.0	23.0	27.0	

Table 3 - Thrust vs. applied-field strength slopes for 3 anode radii and 4 discharge currents. Argon flow rate of 0.10 g/s for 2.54 and 3.81 cm anode, 0.14 for 5.1 cm radius anode.

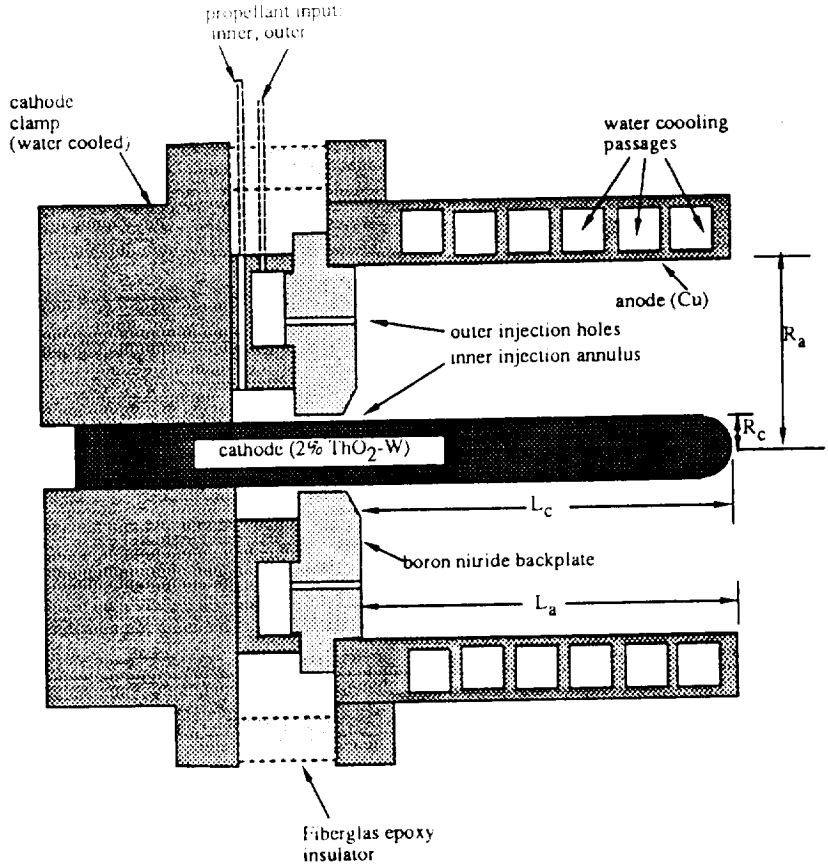

Fig. 1 Schematic of applied-field MPD thrusters used in this test series. Applied-field magnet not shown. Not to scale.

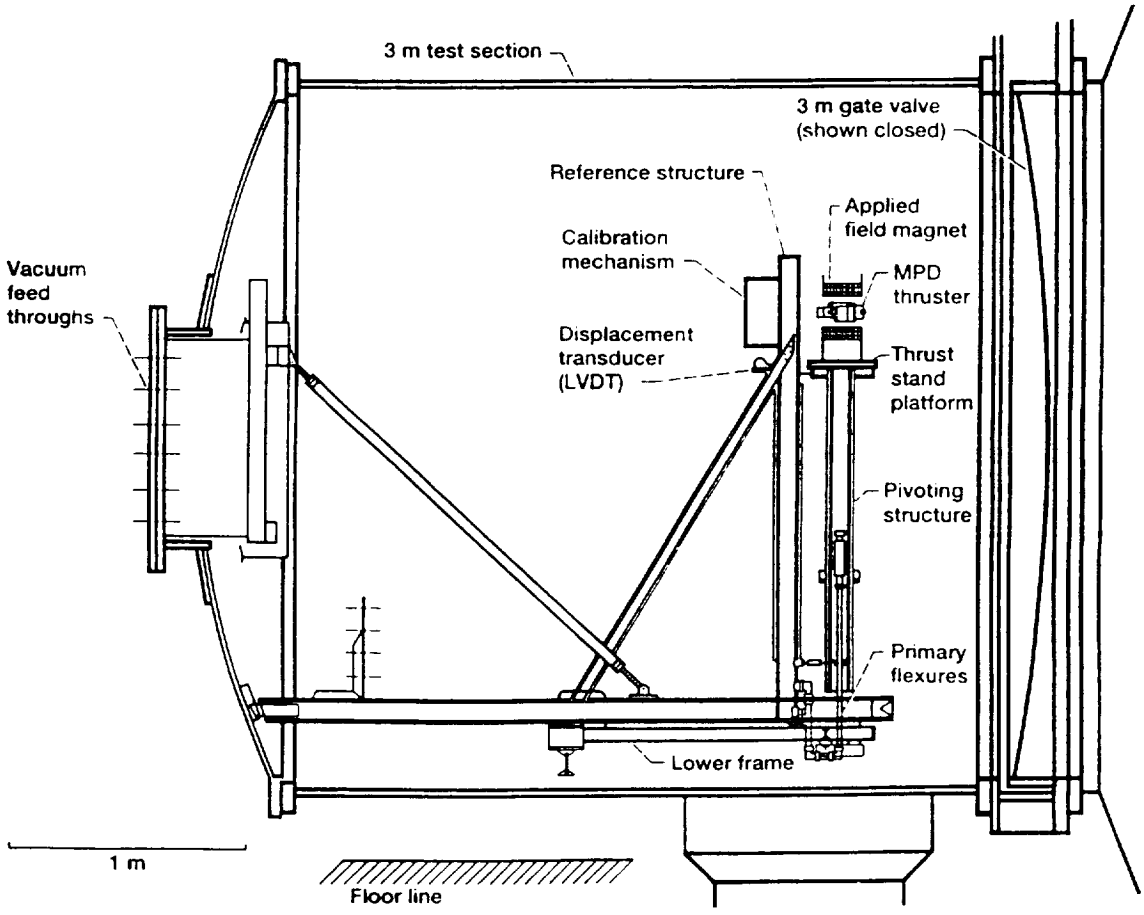

Fig. 2 MPD thruster test stand schematic.

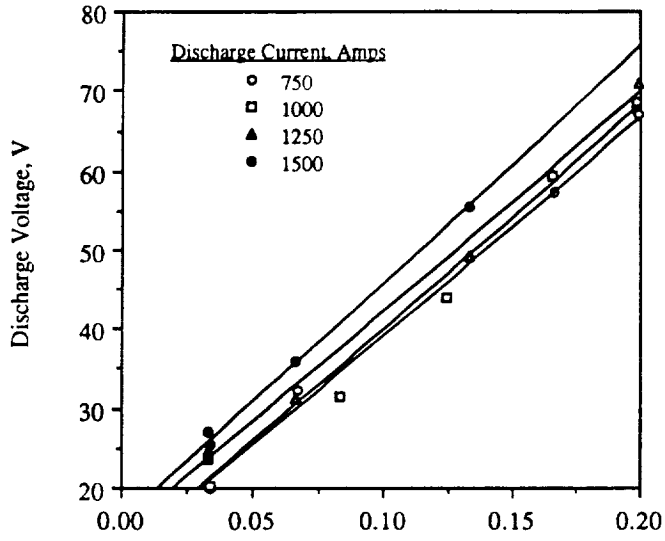

a. 2.5 cm radius anode.

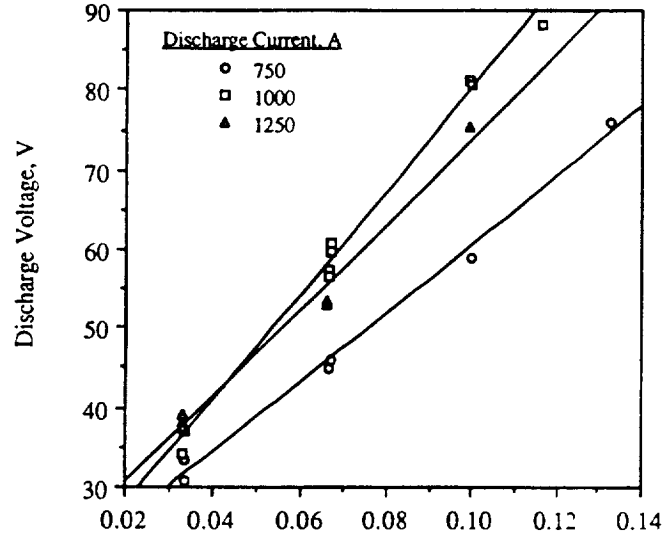

b. 3.81 cm radius anode.

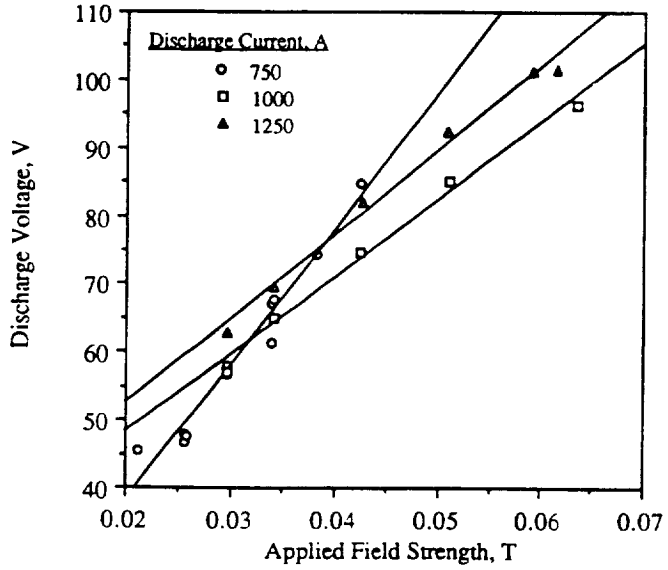

c. 5.1 cm radius anode.

Figure 3 - Discharge voltage vs. applied-field strength for 3 discharge currents with three anode radii. Argon flow rate of 0.10 g/s.

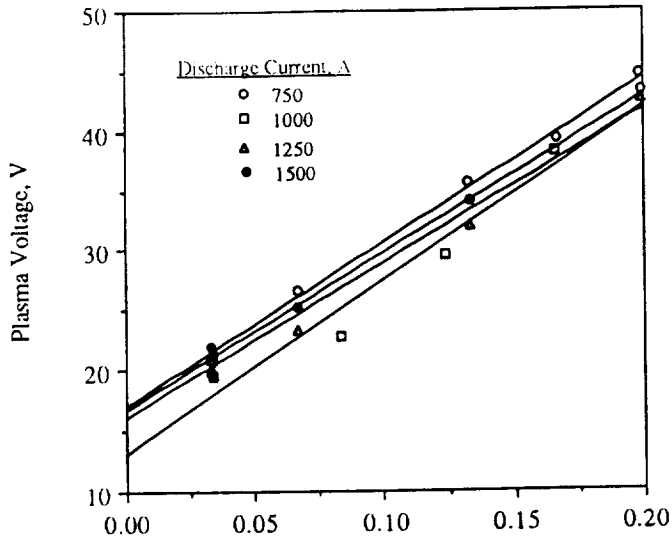

a. 2.5 cm radius anode.

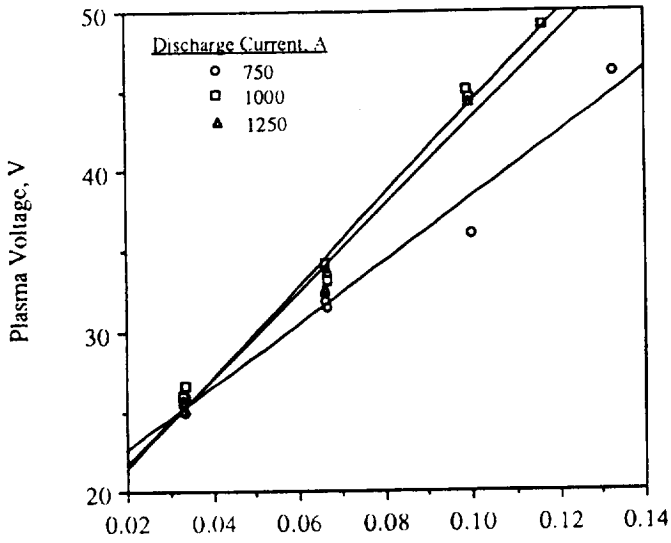

b. 3.81 cm radius anode.

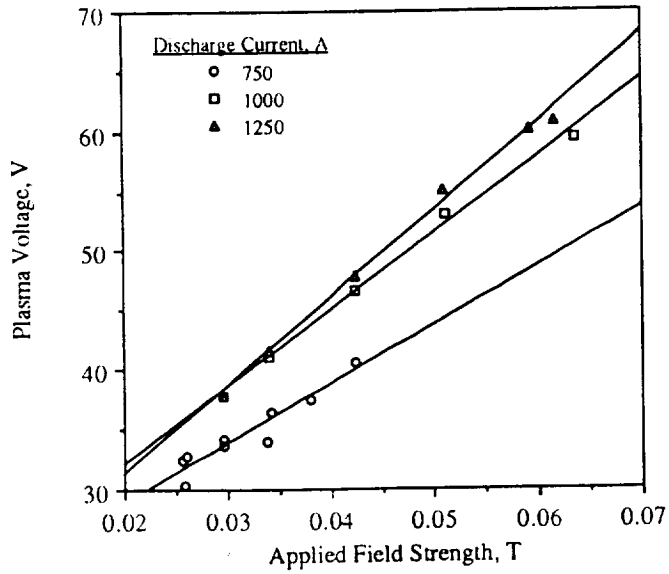

c. 5.1 cm radius anode.

Fig. 4 Plasma voltage vs. applied-field strength for 3 discharge currents with three anode radii. Argon flow rate of 0.10 g/s.

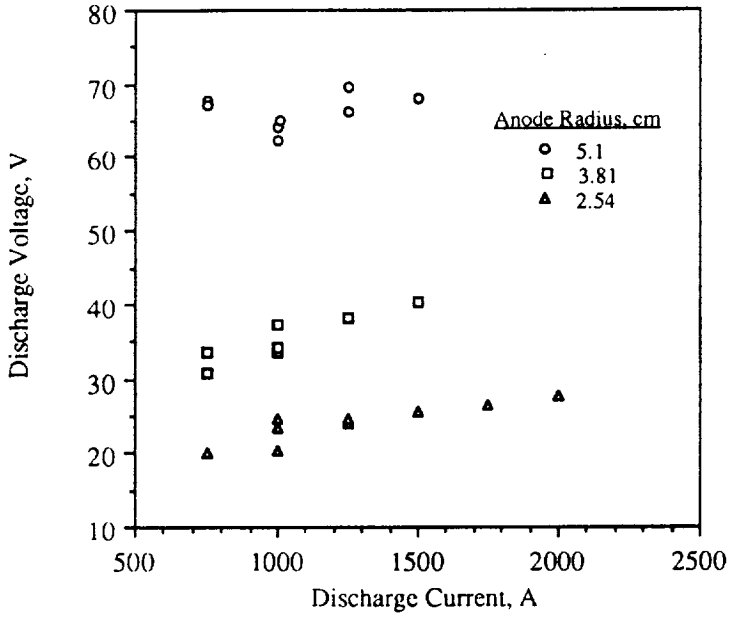

a. Discharge voltage

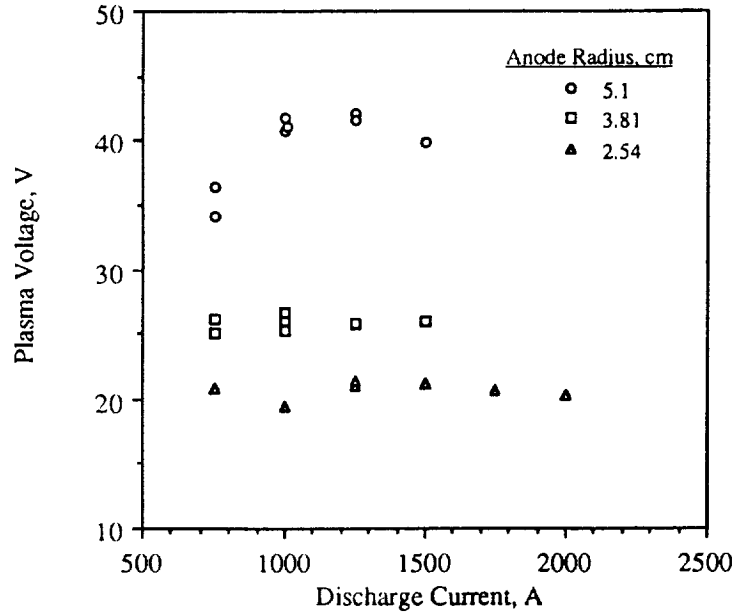

b. Plasma voltage

Fig. 5 Discharge and plasma voltages vs. discharge current for 3 anode radii at an argon flow rate of 0.10 g/s. Applied magnetic field strength of 0.034 T.

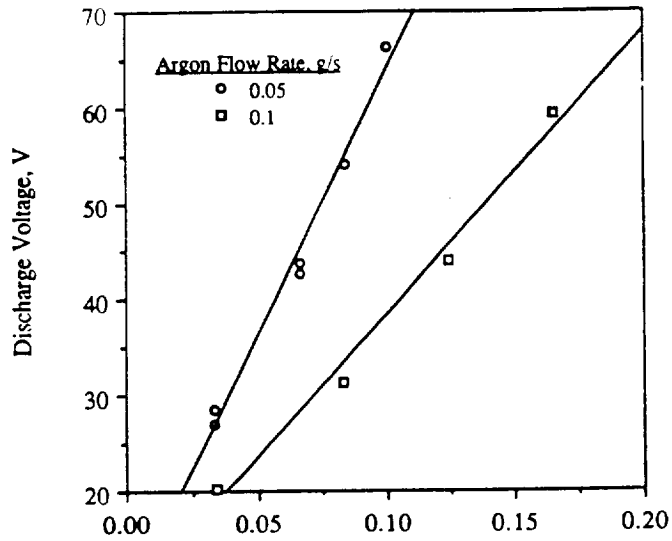

a. 2.54 cm anode radius

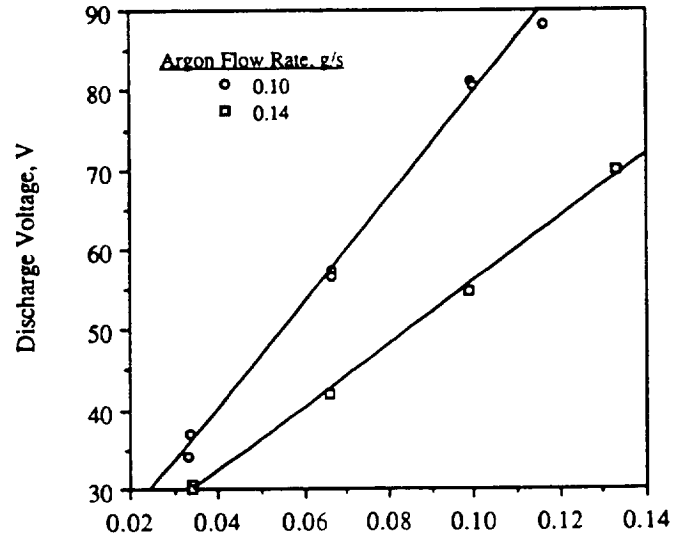

b. 3.81 cm anode radius

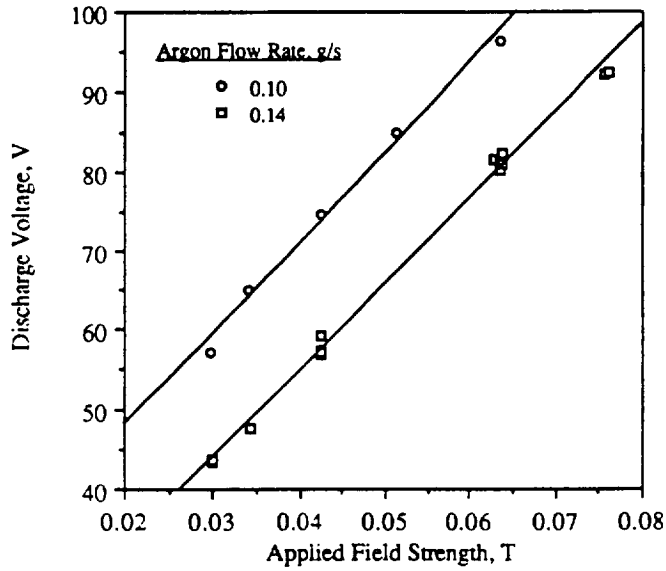

c. 5.1 cm anode radius

Fig. 6 Discharge voltage vs. applied field strength for three anode radii at two argon flow rates and a discharge current of 1000 A.

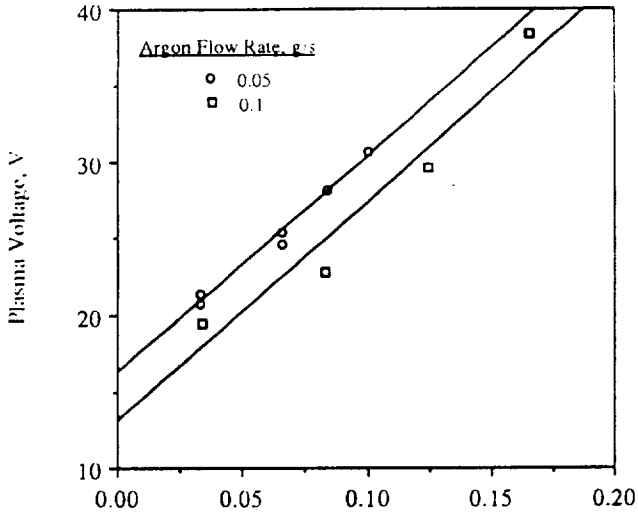

a. 2.54 cm anode radius

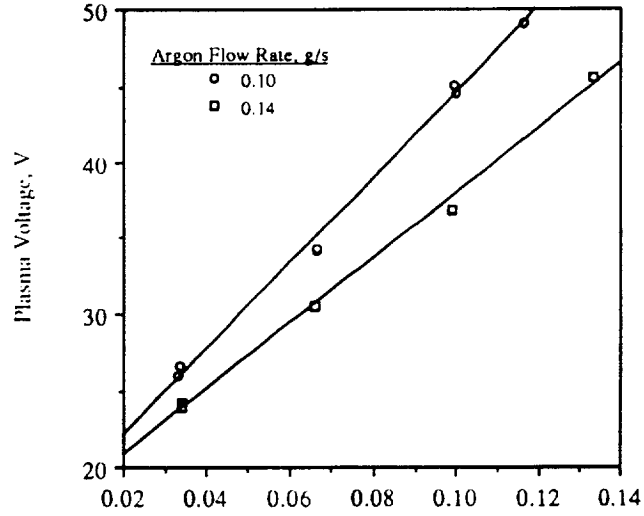

b. 3.81 cm anode radius

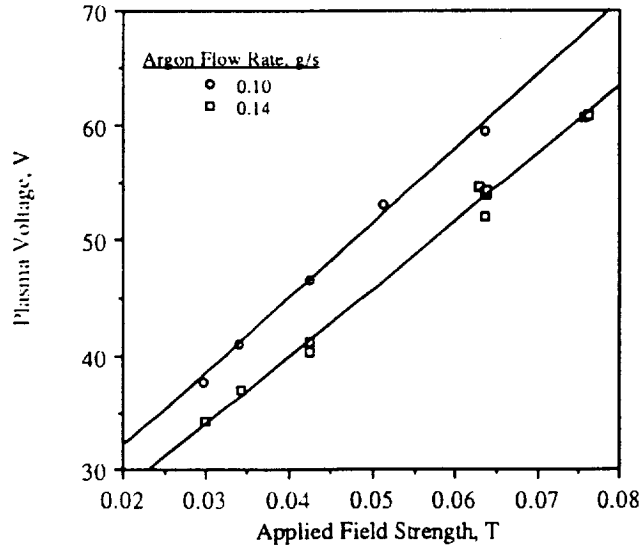

c. 5.1 cm anode radius

Fig. 7 Plasma voltage vs. applied field strength for three anode radii at two argon flow rates and a discharge current of 1000 A.

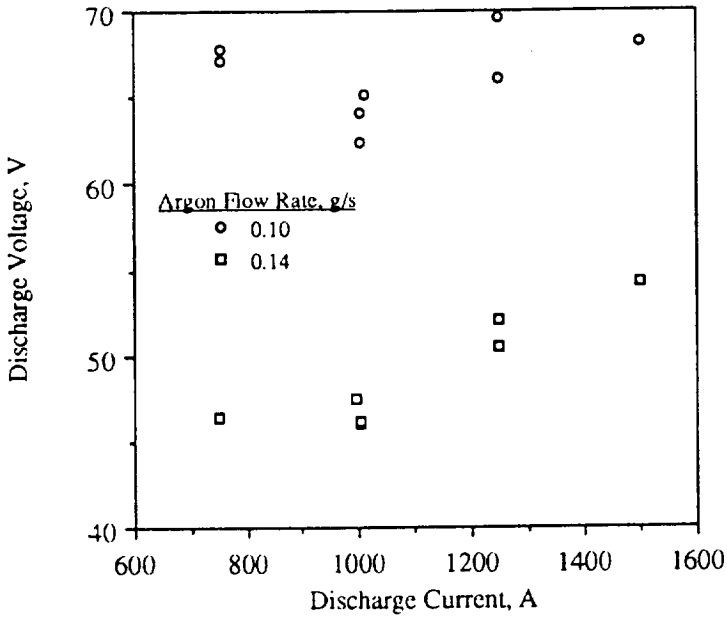

a. Discharge voltage

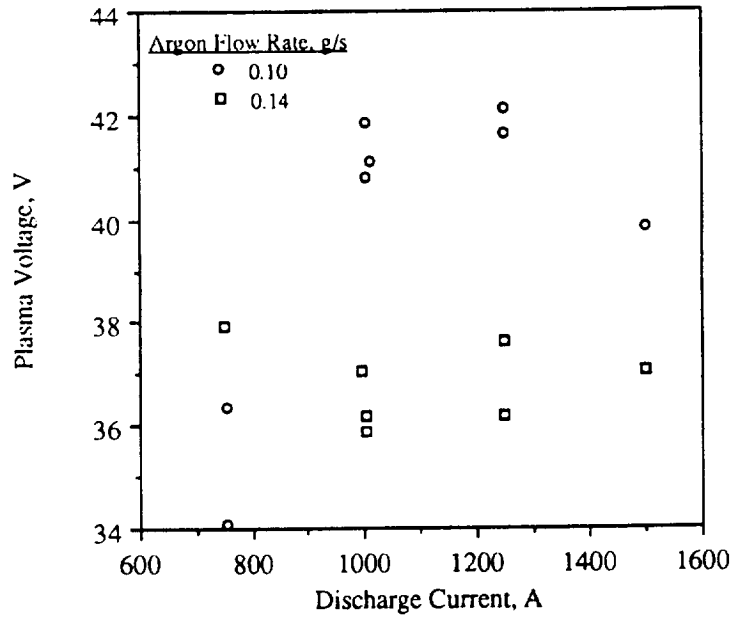

b. Plasma voltage

Fig. 8 Discharge and plasma voltages vs. discharge current for the 5.1 cm radius anode at two argon flow rates with an applied field strength of 0.034 T.

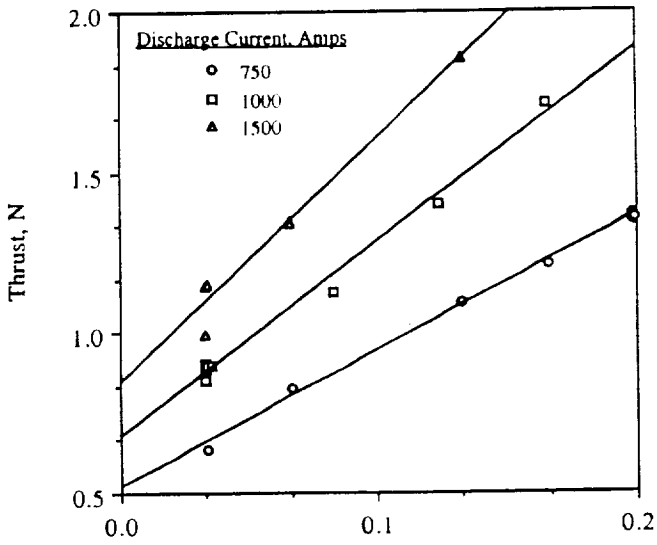

a. 2.54 cm anode radius, 0.10 g/s argon

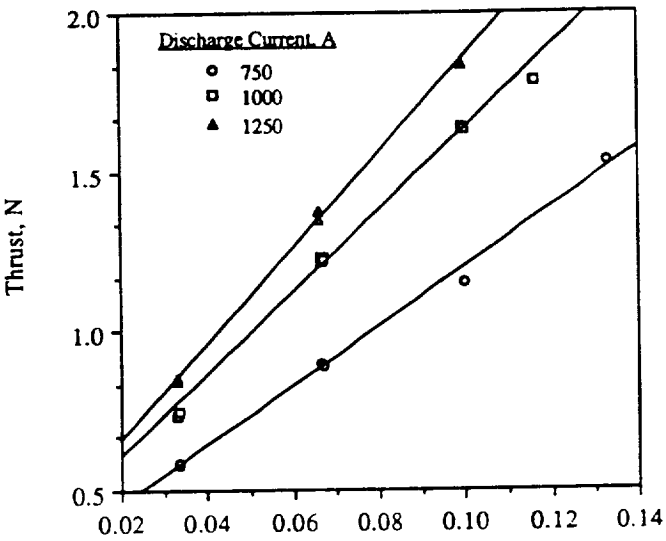

b. 3.81 cm anode radius, 0.10 g/s argon

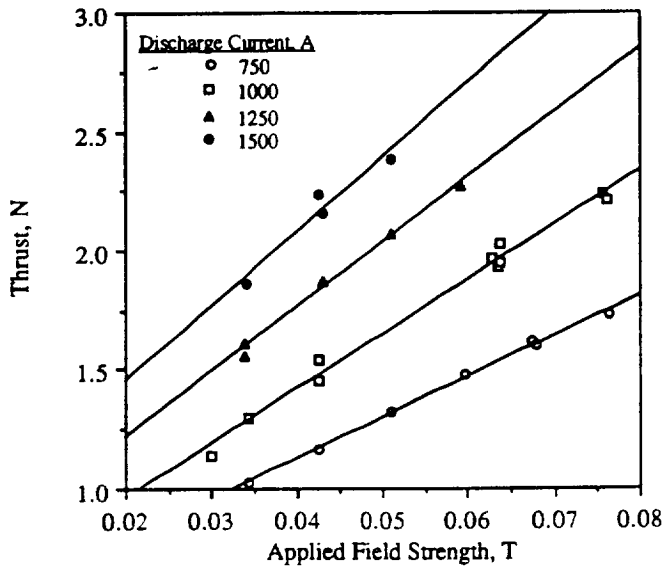

c. 5.1 cm anode radius, 0.14 g/s argon

Fig. 9 Thrust vs. applied field strength for the three anode radii at several discharge currents.

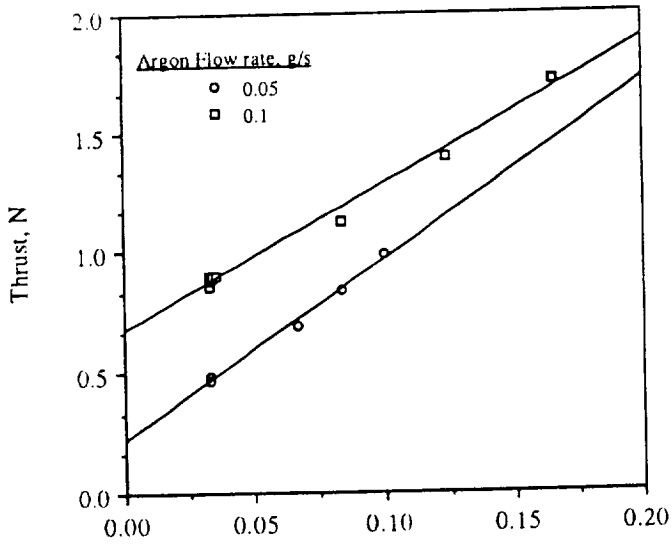

a. 2.54 cm anode radius

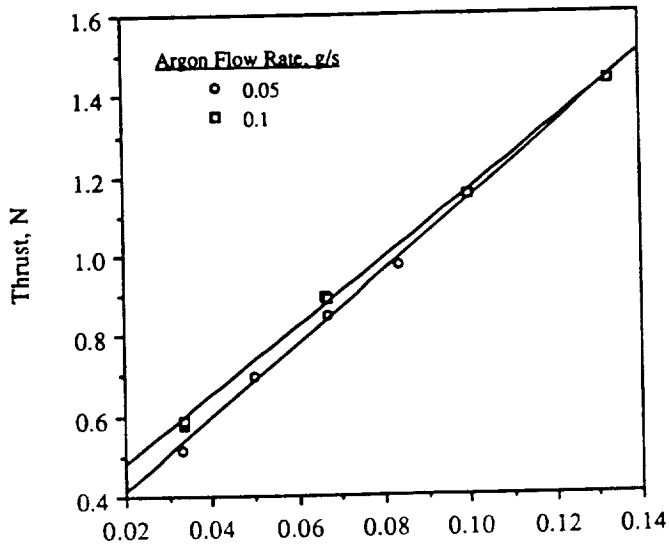

b. 3.81 cm anode radius

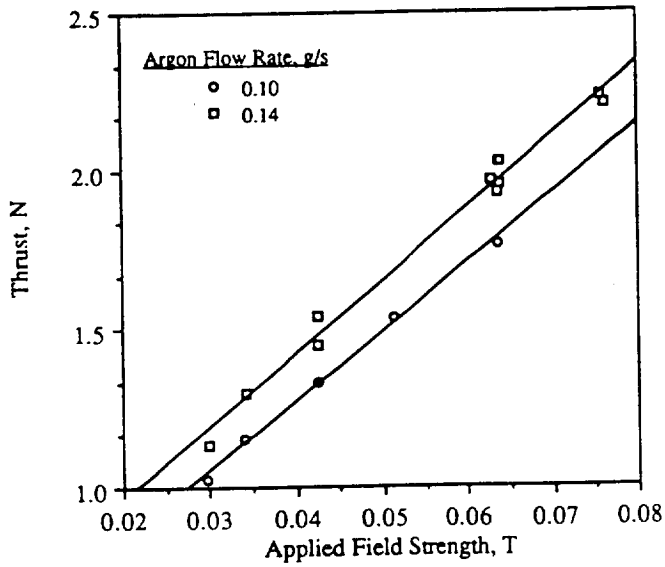

c. 5.1 cm anode radius

Fig. 10 Thrust vs. applied field strength for the three anode radii at 2 argon flow rates. Discharge current of 1000 A.

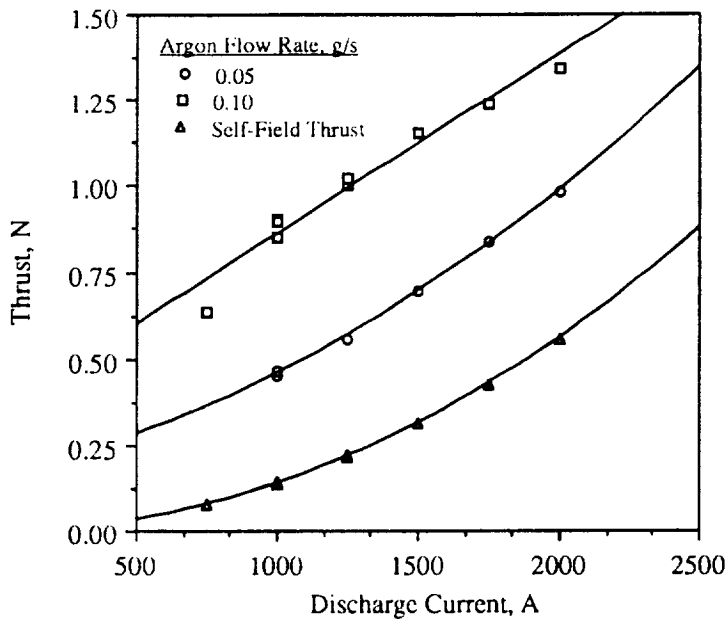

a. 2.54 cm anode radius

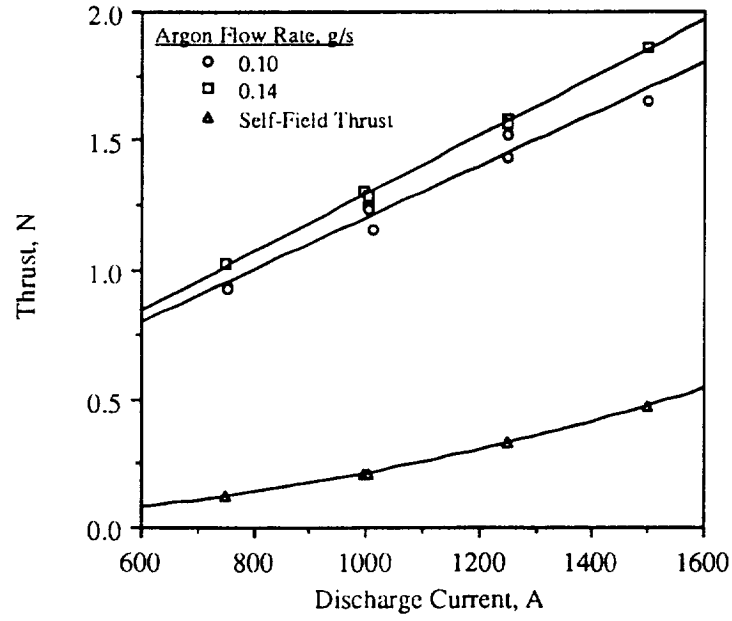

b. 5.1 cm anode radius

Fig. 11 Thrust vs. discharge current for two anode radii at 2 argon flow rates. Calculated self-field thrust also shown. Applied field strength of 0.034 T.

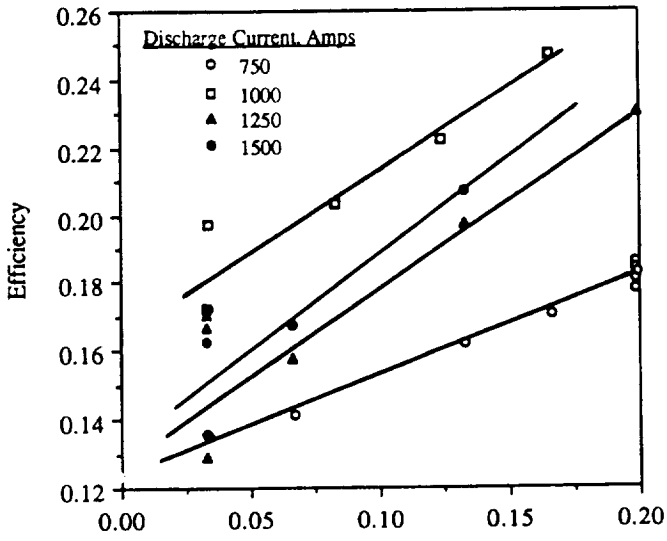

a. 2.54 cm radius, 0.10 g/s argon

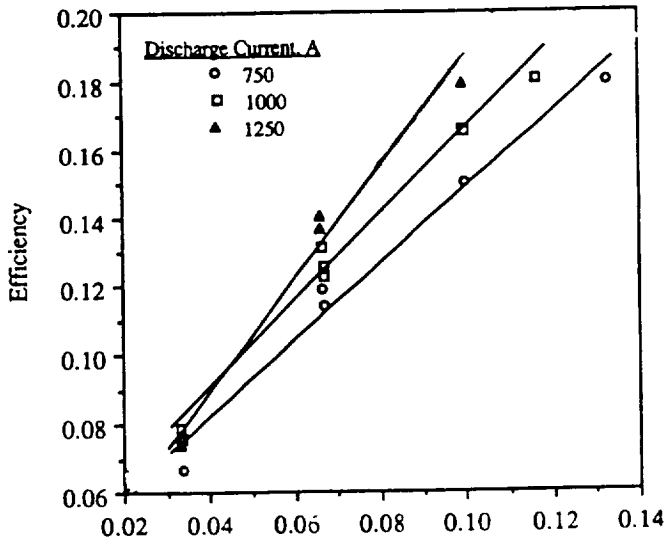

b. 3.81 cm radius, 0.10 g/s argon

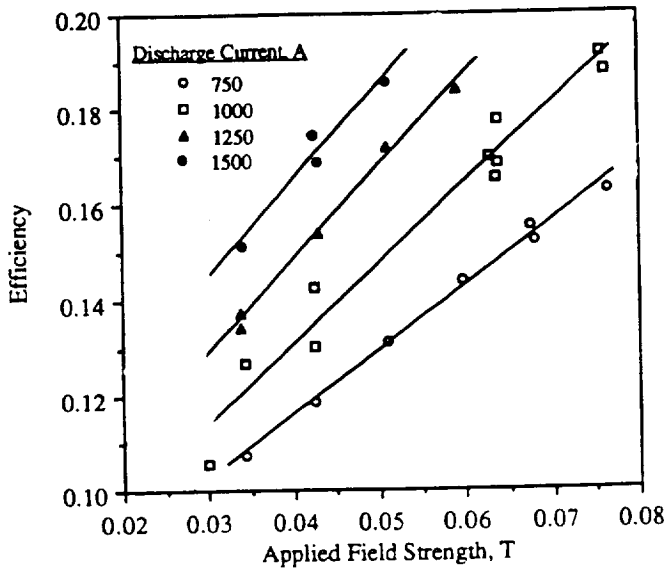

c. 5.1 cm radius, 0.14 g/s argon

Figure 12 - Efficiency vs. applied field strength for 3 anode radii and several discharge currents.

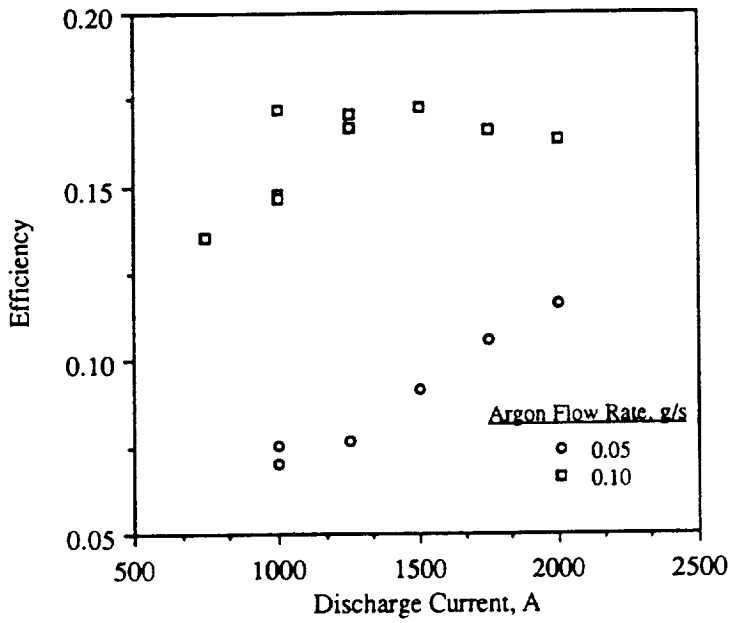

a. 2.54 cm radius

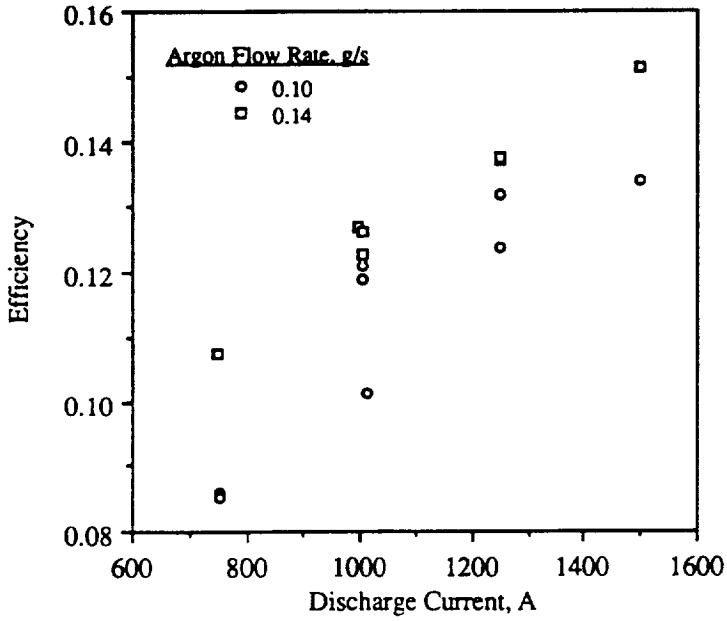

b. 5.1 cm radius

Figure 13 - Efficiency vs. discharge current for 2 anode radii at 2 propellant flow rates. Applied field strength of 0.034 T.

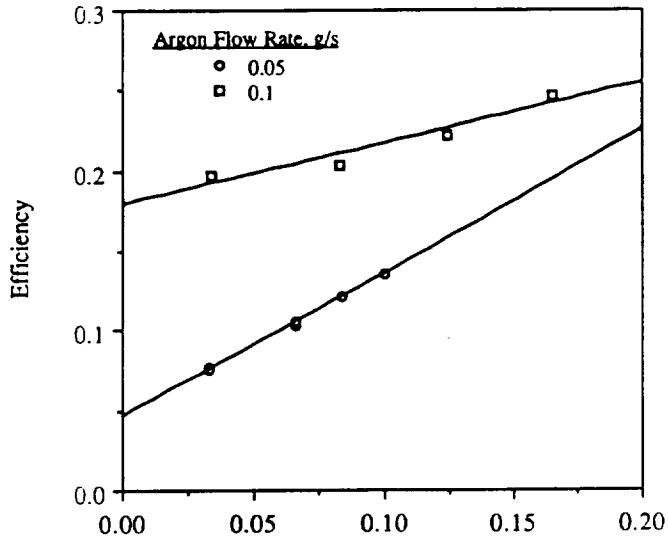

a. 2.54 cm radius

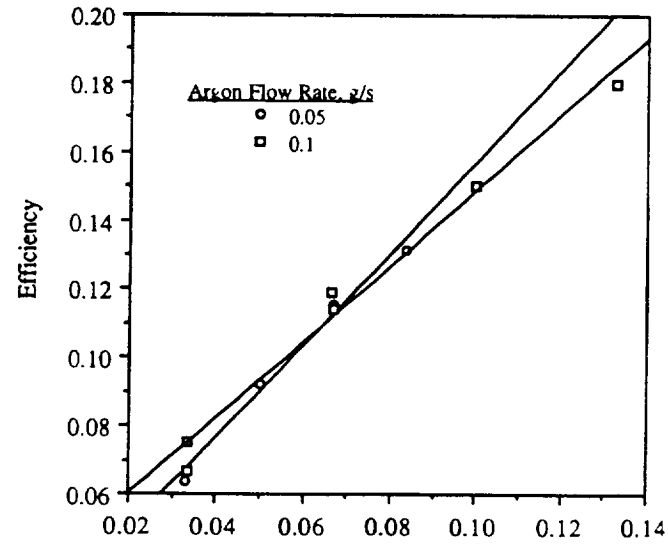

b. 3.81 cm radius

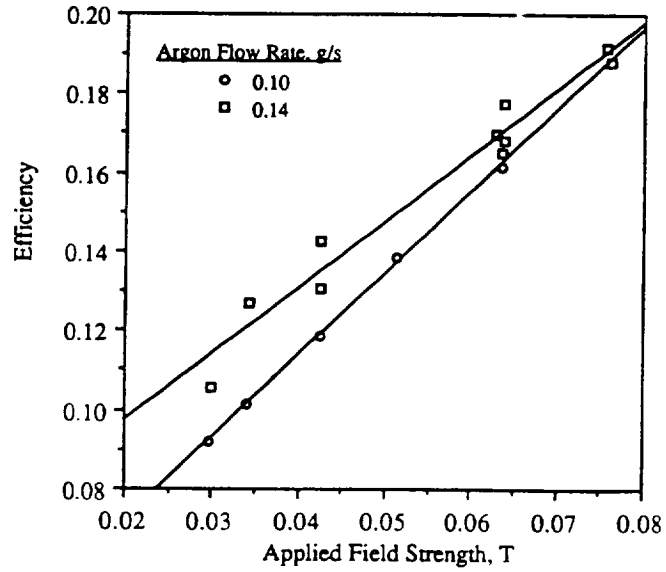

c. 5.1 cm radius

Fig. 14 Efficiency vs. applied field strength for 3 anode radii at 2 propellant flow rates with a discharge current of 1000 A.

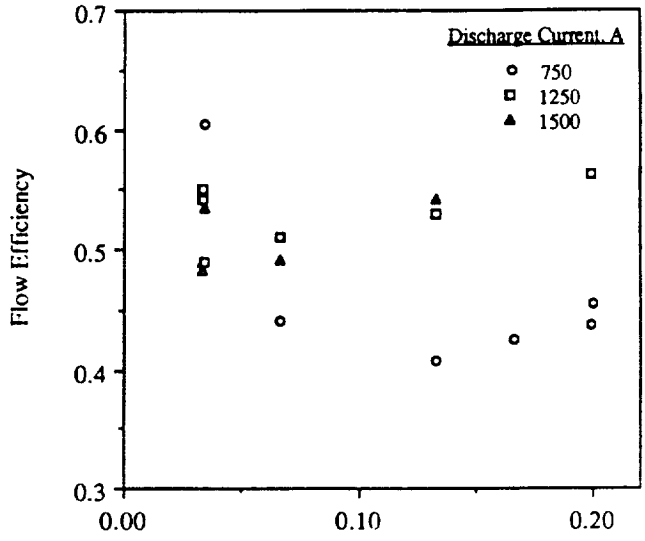

a. 2.54 cm radius, 0.10 g/s

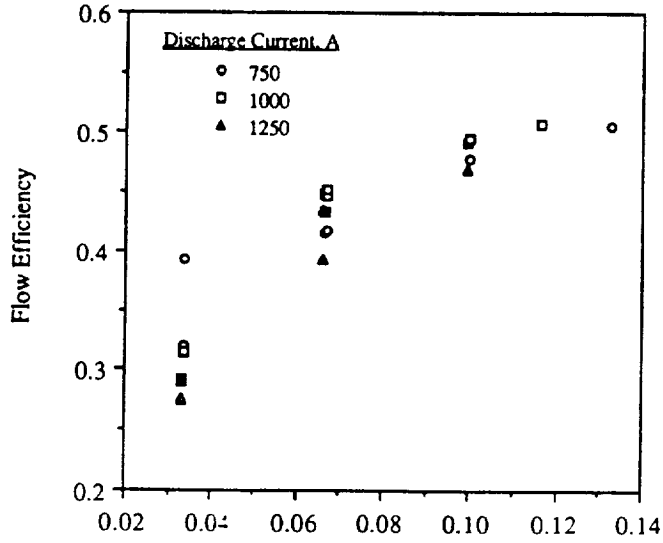

b. 3.81 cm radius, 0.10 g/s

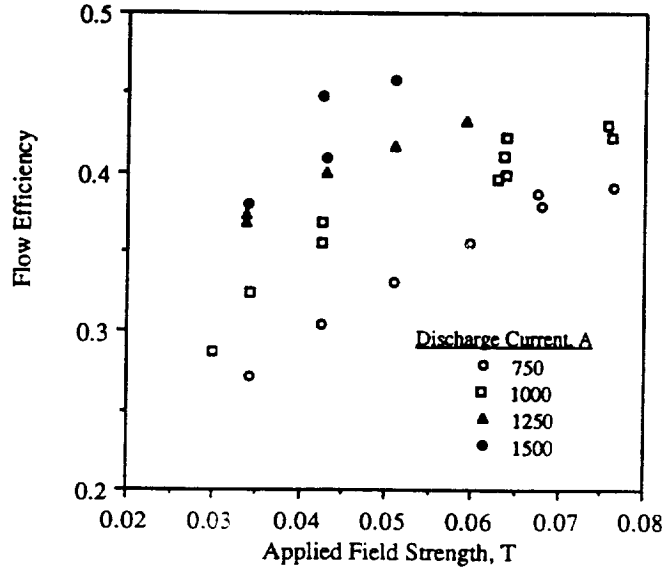

c. 5.1 cm radius, 0.14 g/s

Figure 15 - Flow efficiency vs. applied field strength for 3 anode radii and several discharge currents.

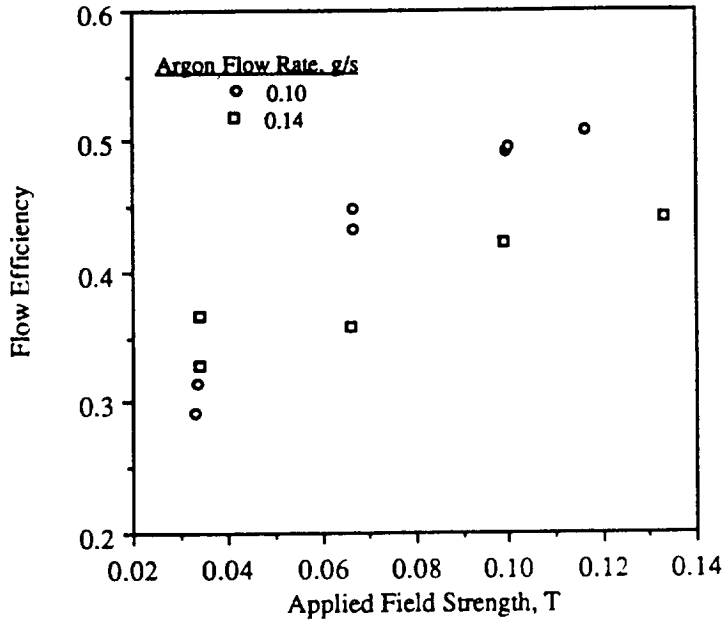

a. 3.81 cm

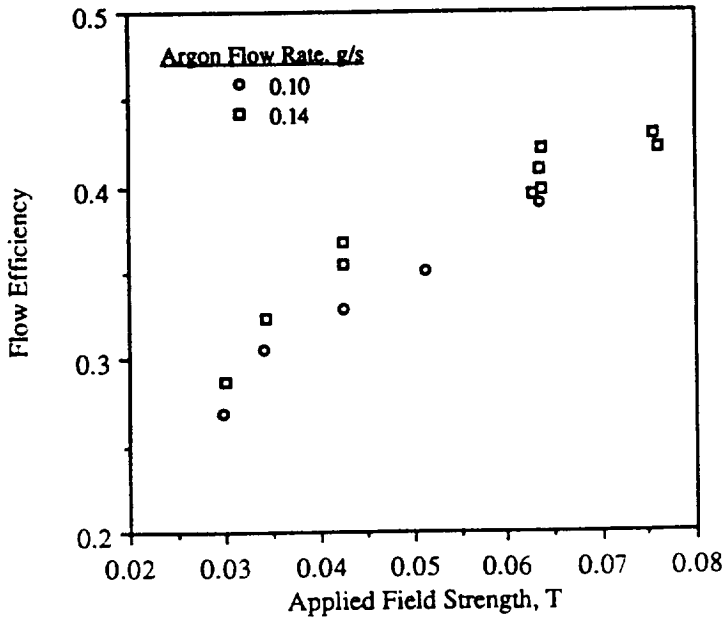

b. 5.1 cm

Fig. 16 Flow efficiency vs. applied field strength for 2 anode radii at two argon flow rates of 0.10 and 0.14 g/s. 1000 A discharge current.

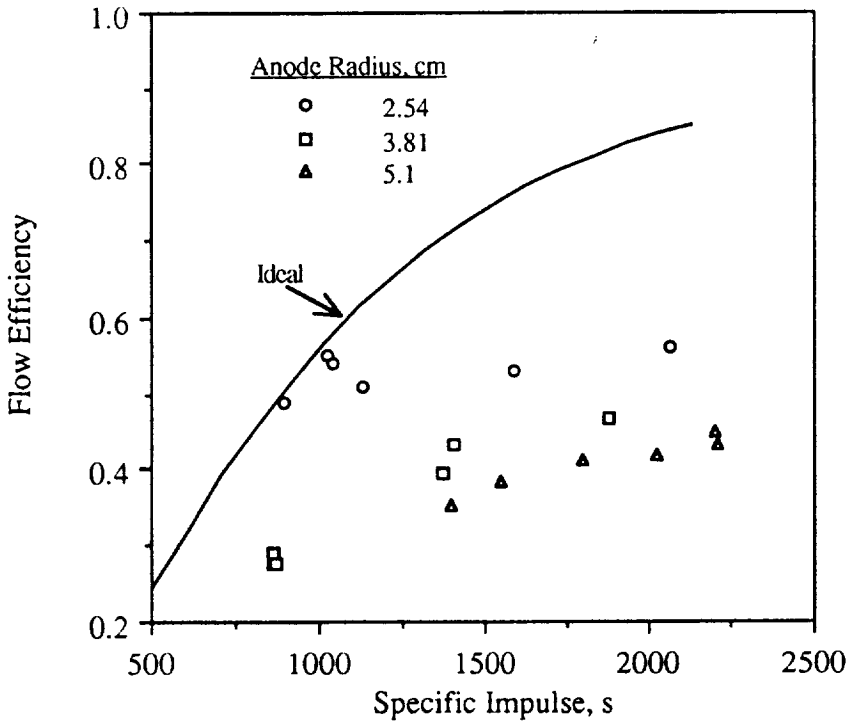

Fig. 17 Ideal and measured flow efficiency vs. specific impulse. Three anode radii, 1250 A discharge current, and 0.10 g/s argon.

REPORT DOCUMENTATION PAGE

Form Approved
OMB No. 0704-0188

1. AGENCY USE ONLY (*Leave blank*)	2. REPORT DATE	3. REPORT TYPE AND DATES COVERED
	July 1992	Final Contractor Report

4. TITLE AND SUBTITLE

Scaling of 100 kW Class Applied-Field MPD Thrusters

5. FUNDING NUMBERS

WU–506–42–31

6. AUTHOR(S)

Roger M. Myers

7. PERFORMING ORGANIZATION NAME(S) AND ADDRESS(ES)

Sverdrup Technology, Inc.
Lewis Research Center Group
2001 Aerospace Parkway
Brook Park, Ohio 44142

8. PERFORMING ORGANIZATION REPORT NUMBER

E–7405

9. SPONSORING/MONITORING AGENCY NAMES(S) AND ADDRESS(ES)

National Aeronautics and Space Administration
Lewis Research Center
Cleveland, Ohio 44135–3191

10. SPONSORING/MONITORING AGENCY REPORT NUMBER

NASA CR–190791
AIAA–92–3462

11. SUPPLEMENTARY NOTES

Project Manager, James S. Sovey, (216) 433–7454.

12a. DISTRIBUTION/AVAILABILITY STATEMENT

Unclassified - Unlimited
Subject Category 20, 75

12b. DISTRIBUTION CODE

13. ABSTRACT ***(Maximum 200 words)***

Three cylindrical applied-field magnetoplasmadynamic thrusters were tested with argon propellant over a broad range of operating conditions to establish empirical scaling laws for thruster performance. Argon flow rates, discharge currents, and applied-field strengths were varied between 0.025 and 0.14 g/s, 750 to 2000 A, and 0.034 to 0.20 T, respectively. The results showed that the thrust reached over five times the self-field value, and that thrust increased linearly with the product of discharge current and applied-field strength and quadratically with the anode radius. While increasing the propellant flow rate increased the thrust, it did not affect the rate of thrust increase with applied-field strength, and at low propellant flow rates the self-field thrust approached 30% of the measured thrust. The voltage increased linearly with applied-field strength was strongly dependent on anode radius. Thruster efficiency increased monotonically with applied-field strength and propellant flow rate. Peak thruster efficiencies were insensitive to changes in anode radius. Electrode power loss and thruster efficiency measurements showed that while the electrode losses decreased with increasing anode radius the plasma losses increased. The opposite behaviors of electrode and plasma losses demonstrates the need to identify ways of independently controlling the thruster loss mechanisms.

14. SUBJECT TERMS

Electric propulsion; Plasma dynamics; Nuclear propulsion

15. NUMBER OF PAGES

30

16. PRICE CODE

A03

17. SECURITY CLASSIFICATION OF REPORT	18. SECURITY CLASSIFICATION OF THIS PAGE	19. SECURITY CLASSIFICATION OF ABSTRACT	20. LIMITATION OF ABSTRACT
Unclassified	Unclassified	Unclassified	